Traveling-Wave Metal-Insulator-Metal Diodes for Infrared Rectennas

Bradley Pelz, Amina Belkadi and Garret Moddel

Department of Electrical, Computer, and Energy Engineering, University of Colorado, Boulder, CO 80309-0425, U.S.A.

***Abstract* — We demonstrate for the first time optical energy conversion using a rectenna incorporating a traveling-wave diode. Optical rectennas use micron sized antennas coupled to high speed diodes to convert an optical wave to DC power. Metal-insulator-metal (MIM) diodes are suitable for high speed operation because of their femtosecond-fast electron tunneling rectification mechanism. However, in a lumped-element rectenna configuration, these devices cannot operate above several terahertz due to their high capacitance. We demonstrate a 10.6 µm (28 THz) MIIM (Ni-NiO-Nb_2O_5-Cr) optical rectenna that incorporates a traveling-wave diode (TWD) geometry to overcome lumped-element diode capacitance limitations.**

I. Introduction

In contrast to conventional semiconductor solar cells, optical rectennas work better for infrared radiation than for visible. For that reason, optical rectennas [1] are natural candidates for long-wavelength cells in spectral splitting solar cells, for waste heat harvesting, and for thermophotovoltaics.

As depicted in Fig. 1, Rectennas absorb electromagnetic radiation in an antenna and couple that energy to a diode. The signal is rectified by the diode, giving DC power out.

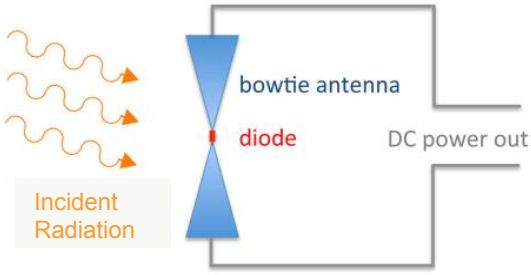

Fig. 1. Optical frequency rectenna.

The standard configuration for an optical frequency MIM rectenna places the MIM diode at the feed point of the antenna, with each antenna arm feeding into opposing sides of the diode. One of the basic requirements for efficient rectenna operation is that the diode cut-off frequency is above the desired operating frequency. Given that resistance scales inversely with area and capacitance scales proportionally to area, the RC time constant is independent of diode area. With the additional restriction that the diode impedance needs to match the antenna impedance of ~100 Ω [2], and the relatively high capacitance associated with the parallel plate configuration of an MIM diode, lumped-element MIM rectennas cannot operate above several terahertz [3].

One option for overcoming the frequency limitation of a lumped-element MIM rectenna, that still takes advantage of the femtosecond-electron tunneling in MIM tunnel junctions [4], is to use a traveling-wave diode (TWD) MIM geometry. This structure was patented in 2006 [5], and demonstrated as a waveguide-coupled detector a year later [6]. Simulations have shown that for a rectenna operating as a detector the TWD configuration provides substantially better performance in the near infrared than a lumped-element diode [7]. In this configuration both antenna arms feed into the same side of the structure to launch a surface plasmon mode down the transmission line structure, such that the impedance seen by the antenna is the characteristic impedance. Because this characteristic impedance can be tuned to be mostly real and matched to the antenna, a TWD is a good option for infrared energy harvesting. Fig. 2 illustrates how a bowtie antenna couples to the TWD and how the surface plasmons propagate down the structure.

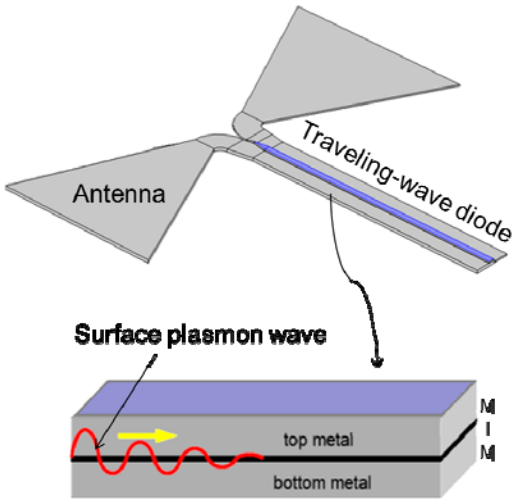

Fig. 2. Traveling-wave diode rectenna, and section of overlap region that forms the diode. A decaying surface plasmon is shown propagating and decaying down the length of the structure.

II. Traveling-Wave Diode Operation

A. TWD Concept

The TWD is essentially a rectifying transmission line for surface plasmons. One end of the TWD is connected to a bowtie antenna. When the antenna is excited by an

electromagnetic wave, the energy concentrates at the feed point of the antenna. From there it launches a coupled surface plasmon wave down the MIM interface. An MIM interface supports two propagation modes, symmetric and antisymmetric. The antisymmetric mode, having the electric field profile shown in Fig. 3, is the only mode that is supported in the infrared [8]. The strong field confinement in the insulator and perpendicular to the MIM interface is responsible for driving the electron tunneling which, just as with a lumped-element MIM diode, is the rectification mechanism of the TWD rectenna.

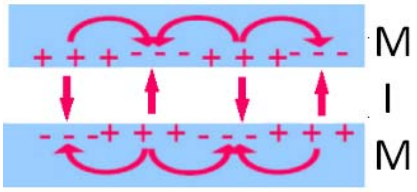

Fig. 3. Electric field profile for antisymmetric mode surface plasmon at an MIM interface.

B. Simulation

Simulations of the device using COMSOL Multiphysics confirmed that the bowtie antenna launches a surface plasmon mode down the MIM interface, and that the wave is expected to be the antisymmetric mode necessary to drive electron tunneling and rectification. Additionally, COMSOL allowed us to estimate the TWD characteristic impedance and showed us the impedance is dominantly real. Therefore, the effect of the small reactive component can be ignored, and the coupling efficiency, η_C [3], with antenna resistance R_A and diode resistance R_D, is

$$\eta_C \equiv 4\frac{R_A R_D}{(R_A + R_D)^2} \qquad (1)$$

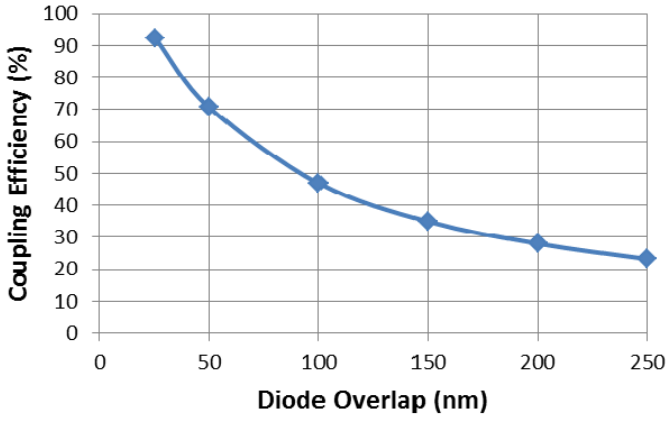

Fig. 4. TWD coupling efficiency with a 100 Ω antenna vs. the TWD width.

COMSOL simulations indicated that one key parameter for adjusting the diode characteristic impedance is the diode overlap width. Using impedance estimates from COMSOL and (1), we plot the coupling efficiency vs. the TWD overlap width in Fig. 4. As can be seen in the plot, to obtain a high coupling efficiency the traveling-wave region must be narrow. We thus targeted a TWD width of ~100 nm.

III. Fabrication

To meet the 100 nm feature size necessary for a successful impedance match of the TWD to the antenna, we use a modified germanium shadow mask process that allows for a single, self-aligned mask layer [6].

The first step in the germanium shadow mask process is to spin coat a 280 nm layer of PMMA on a silicon wafer coated with a thermally grown SiO_2 layer. Next, a 60 nm layer of germanium is thermally evaporated. Using an ASML S500/300 DUV stepper, a pattern like the one shown in the upper right corner of Fig. 5 is printed on the wafer. Using a CF_4 etch, the pattern is transferred into the germanium. The subsequent O_2 plasma etch removes the exposed PMMA and undercuts the germanium bridge, exposing the substrate below.

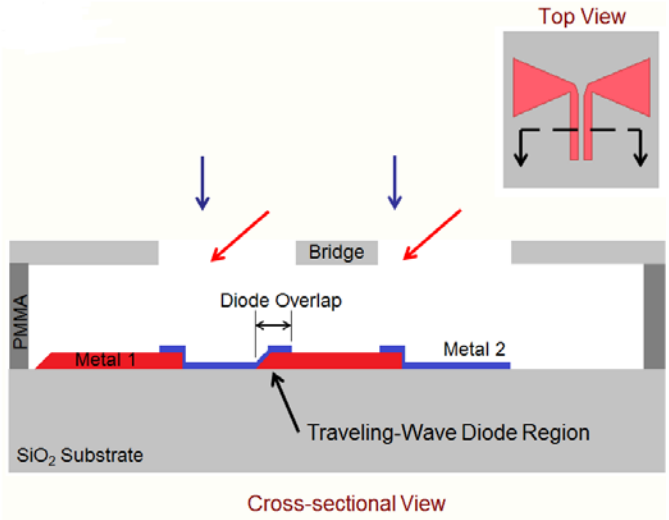

Fig. 5. Cross-section view and top view of germanium shadow mask fabrication of a traveling-wave diode.

The cross-section of the germanium bridge shown in Fig. 5 is suspended over the wafer surface by unetched PMMA out of the plane of the cross-section. At this point, the germanium shadow mask is complete and the device fabrication can begin.

For our devices, we decided to use a modified version of an MIM diode, the MIIM diode that includes a second insulator to improve the diode nonlinearity and asymmetry [9]. Our chosen MIIM material set was Ni-NiO-Nb_2O_5-Cr. The relatively low dielectric constant for NiO improves the transmission characteristics of the coupled surface plasmon

mode along the TWD compared to higher dielectric insulators. Experimental DC measurements showed that Nb_2O_5 and Cr paired well with the Ni-NiO base to give an asymmetric I(V) characteristic. The first metal layer, nickel, was thermally evaporated at an angle of 43° from the right. Next a thin NiO film, ~3 nm, was grown in an oxygen plasma and a thin, ~2 nm, Nb_2O_5 was sputter deposited. Finally, the second metal, chromium, was evaporated at normal incidence. The cross section in Fig. 5 shows that seven distinct regions are expected in the transmission line section of the TWD. Two regions contain only the first metal, two contain only the second metal, and three regions involve both. The center region with both metals is the traveling-wave diode overlap.

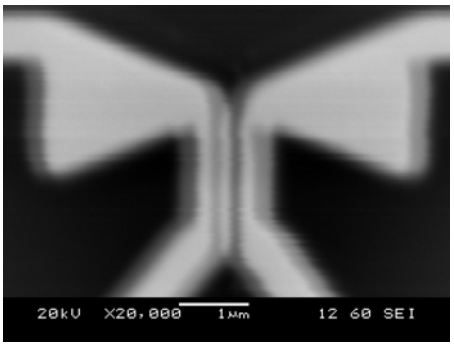

Fig. 6. Scanning electron microscope image of TWD.

The scanning electron microscope image in Fig. 6 shows the final TWD after liftoff. As expected from Fig. 5, there are seven distinct regions in the transmission line structure, with the center bright strip being the MIM TWD overlap region. Based on this SEM image, the overlap was measured to be ~115 nm, achieving the design specifications. For this width, the estimated TWD characteristic impedance is ~14 Ω. Despite a TWD characteristic impedance nearly an order of magnitude lower impedance than the ~100 Ω antenna, using (1) the estimated coupling efficiency is 43%.

IV. Experimental

A. DC Characterization

Prior to any optical measurements, we obtained the DC I(V) characteristics of our TWD using a four-point probe measurement. In Fig. 7 we show the differential diode resistance and diode responsivity. The responsivity is a measure of the DC current out as a function of AC power in, and is defined as:

$$\beta \equiv \frac{1}{2}\frac{I''}{I'} \qquad (2)$$

The DC characterization of this devices shows that the MIM interface is in fact asymmetric, with a zero bias responsivity of -0.66 A/W. Having an asymmetric tunnel junction is important for two reasons: First, having an asymmetric device eliminates the need for a bias voltage which would make it difficult to distinguish a rectification from a bolometric optical response [10]. Second, while a biased symmetric device can work as a detector, it cannot function as an energy harvester.

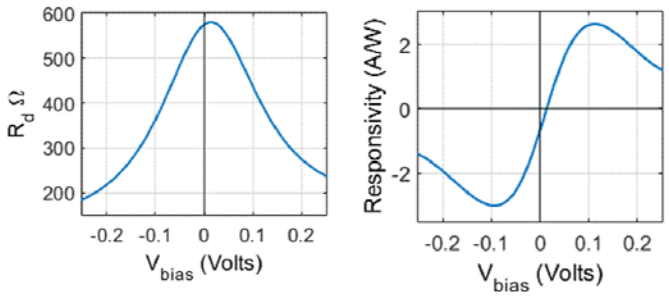

Fig. 7. Resistance and responsivity characteristics from DC I(V) measurement.

B. Optical Measurements

To experimentally confirm the infrared operation, we measured the TWD rectenna under illuminated with a linearly polarized SYNRAD 48-1SWJ IR CO_2 laser (10.6 μm). The laser has a maximum intensity at the beam center of 1 x 10^5 W/m^2. The beam passed through a mechanical chopper to provide for lock-in (Stanford Research Systems SR830) detection in measuring the open circuit voltage from the rectenna. The beam also passed through a half-wave plate to allow the polarization of the beam to be rotated relative to the antenna axis.

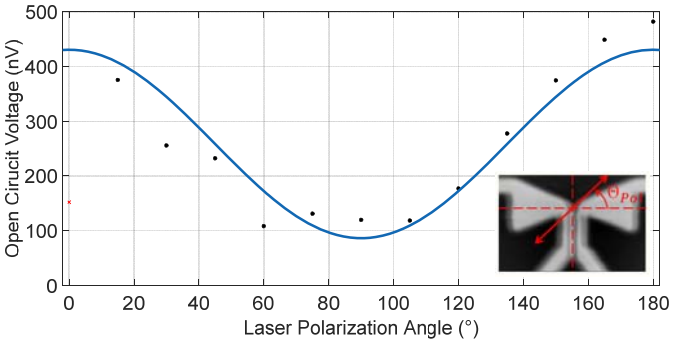

Fig. 8. Open circuit voltage polarization response (black dots) for the MIM traveling-wave diode and fit (blue line). Note: 0° polarization data omitted due to shutter malfunction.

As expected, Fig. 8 shows that when the beam polarization is aligned with the antenna axis (0° and 180°), the response is maximized. Conversely, when the illumination polarization is perpendicular to the antenna axis (90°), the rectenna response is a minimum. We expect the data to fit a $\cos^2(\theta)$ dependence on polarization angle, where minimum signal at 90° reaches zero. Contrary to this expectation, the minimum response does not go to zero. We believe this is due to direct absorption in the traveling-wave structure, which is orientated perpendicular

to the antenna axis and of similar dimensions to the antenna. This direct absorption cannot excite the surface plasmon mode necessary for rectification; however, it can result in Joule heating of the junction and a Seebeck voltage similar to the results found by Bareiß, et al. [11]. Given this additional absorption mechanism, the fit equation required an additional, polarization dependent, $\sin^2(\theta)$ term for the orthogonal absorption in the traveling-wave structure where θ is the laser polarization angle relative to the antenna axis. The optical response data was fit using (3), where V_{OC} is the illuminated rectenna open circuit voltage, A_{Rec} is the coefficient of the rectification response due to absorption in the antenna coupling to the TWD, and A_{Th} is the coefficient of the thermal response from the absorption in the traveling-wave structure.

$$V_{OC} = A_{\mathrm{Rec}} \cos^2(\Theta) + A_{Th} \sin^2(\Theta) \qquad (3)$$

The fit from (3) gives the coefficients for the rectification (A_{Rec} = 431 nV) and thermal (A_{Th} = 86 nV) responses with an adjusted R-squared value of 0.88. R-squared. R-squared is the coefficient of determination and provides a metric describing the quality of the fit.

The thermal response of this structure was confirmed by fabricating similar TWD structures without the insulators of the MIM. Without the insulator, these devices form metal-metal junctions and have linear I(V) characteristics. We measured these devices with the same illumination setup as the MIM devices, and fit the data to (3). The fit gives the coefficients for the rectification (A_{Rec} = 14 nV) and thermal (A_{Th} = 68 nV) responses with an adjusted R-squared value of 0.82. The rectification coefficient is at the noise level, so the response is entirely thermal. This additional result supports our choice to fit our optical response from the MIM TWD with (3).

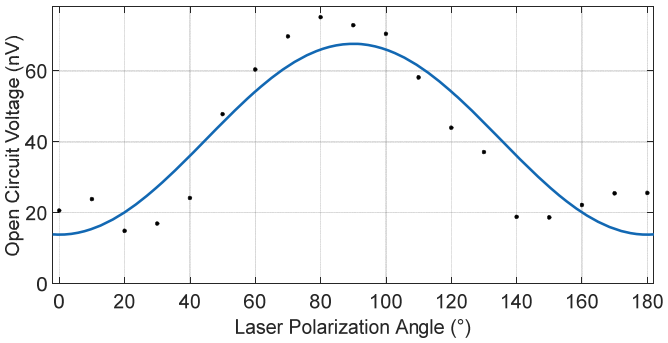

Fig. 9. Open circuit voltage polarization response (black dots) for metal-metal junction traveling-wave device and fit (blue line).

Taking the measured rectification open circuit voltage of 431 nV, and using the diode resistance, 580 Ω, the approximate short circuit current is calculated to be 743 pA. The power into the rectenna can be estimated based on the illumination intensity of 1 x 10^5 W/m^2 and the approximate absorption area of the bowtie antenna, 3.6 x 10^{-11} m^2, giving an optical input power of 3.6 µW. The losses are consistent with simulated device performance.

V. Future Work

This demonstration shows that the TWD rectenna can harvest 10.6 µm infrared light, which cannot be achieved by a rectenna based on lumped-element MIM diodes [3]. Much improvement is needed to provide practical energy harvesting devices. To improve the efficiency, MIM diode materials need to be incorporated that provide substantially improved responsivity near zero volts. Coupled rectennas arrays will increase the total output power.

VI. Summary

We demonstrated an MIM rectenna harvesting power from infrared light at 28 THz (10.6 µm). To overcome the frequency limitation imposed by the RC time constant for a lumped-element MIM diode, we designed and incorporated an MIM rectifying transmission line structure that is tunable to match the antenna impedance. The dependence of the output voltage on the polarization of the input optical beam is consistent with the dominant response being due to rectification along with a smaller response due to a thermal Seebeck voltage.

Acknowledgements

This work was funded by a contract from RedWave Energy Inc. We thank David Doroski for fabrication assistance, and Brad Herner and Shuai Yuan for helpful discussion. The third author holds stock in RedWave Energy Inc.

References

[1] R. L. Bailey, “A proposed new concept for a solar-energy converter,” *Journal of Engineering for Power,* no. 73, April 1972

[2] A. Sanchez, C. F. Davis, K. C. Liu, and A. Javan, "The MOM tunneling diode: Theoretical estimate of its performance at microwave and infrared frequencies," J. Appl. Phys., vol. 49, no. 10, pp. 5270-5277, 1978.

[3] S. Grover and G. Moddel, “Applicability of metal/insulator/metal (MIM) diodes to solar rectennas,” *IEEE Journal of Photovoltaics*, vol. 1, no. 1, pp. 78 –83, Jul. 2011.

[4] M. Nagae, “Response time of metal-insulator-metal tunnel junctions,” *Jpn. J. Appl. Phys.,* vol. 11, no. 11, pp. 1611-1621, Nov. 1972

[5] Estes MJ, Moddel G. Surface plasmon devices. US Patent 7,010,183. 2006

[6] Hobbs, Philip C. D., Robert B. Laibowitz, Frank R. Libsch, Nancy C. Labianca, and Punit P. Chiniwalla. "Efficient waveguide-integrated tunnel junction Detectors at 1.6 µm." *Opt. Express Optics Express* 15.25 (2007)

[7] S. Grover, O. Dmitriyeva, M. Estes, and G. Moddel, "Traveling-wave metal/insulator/metal diodes for improved infrared

bandwidth and efficiency of antenna-coupled rectifiers," IEEE Transactions on Nanotechnology 9.6 (2010)

[8] Woolf, David, Marko Loncar, and Federico Capasso. "The forces from coupled surface plasmon polaritons in planar waveguides." *Optics Express* 17.22 (2009)

[9] Grover, Sachit, and Garret Moddel. "Engineering the current–voltage characteristics of metal–insulator–metal diodes using double-insulator tunnel barriers." *Solid-State Electronics* 67 (2012): 94-99.

[10] Codreanu, Iulian, Francisco J. Gonzalez, and Glenn D. Boreman. "Detection mechanisms in microstrip dipole antenna - coupled infrared detectors." *Infrared Physics & Technology* 44 (2003): 155-63.

[11] Bareiß, Mario, Peter M. Krenz, Gergo P. Szakmany, Badri N. Tiwari, Daniel Kälblein, Alexei O. Orlov, Gary H. Bernstein, Giuseppe Scarpa, Bernhard Fabel, Ute Zschieschang, Hagen Klauk, Wolfgang Porod, and Paolo Lugli. "Rectennas revisited." *IEEE Transactions on Nanotechnology* 12.6 (2013): 1144-150.